Journal of Solid Mechanics Vol. 10, No. 1 (2018) pp. 98-109

Improving Power Density of Piezoelectric Vibration-Based Energy Scavengers

R. Hosseini [1,*], O. Zargar [2], M. Hamedi [3]

[1] *Young Researchers and Elite Club, South Tehran Branch, Islamic Azad University, Tehran, Iran*
[2] *School of Mechanical Engineering, College of Engineering, University of Tehran, Tehran, Iran*
[3] *Department of Mechanical Engineering, Faculty of Engineering, University of Tehran, Iran*

Received 27 September 2017; accepted 14 December 2017

ABSTRACT

Vibration energy harvesting with piezoelectric materials currently generate up to 300 microwatts per cm^2, using it to be mooted as an appropriate method of energy harvesting for powering low-power electronics. One of the important problems in bimorph piezoelectric energy harvesting is the generation of the highest power with the lowest weight. In this paper the effect of the shape and geometry of a bimorph piezoelectric cantilever beam harvester on the electromechanical efficiency of the system is studied. An analytic model has been presented using Rayleigh cantilever beam approximations for piezoelectric harvesters with tapered bimorph piezoelectric cantilever beam. In order to study the effect of a cantilever beam length and geometry on the generated voltage, finite element simulation has been performed using ABAQUS. Design optimization has been used to obtain the maximum output power and tapered beams are observed to lead to more uniform distribution of strain in the piezoelectric layer, thus increasing efficiency.

Keywords: Vibration energy harvesting; Piezoelectric; Power scavenger; Natural frequency; Design optimization.

1 INTRODUCTION

ENERGY harvesting is to provide energy using the surrounding environment and its conversion into the required electric energy. Energy harvesting have been discussed for decades in macro and micro scales for application in different equipment. In order to supply the global demands for energy, processing systems have been successfully built on large scales. On the other hand, for low-power equipment, energy harvesting from the environment is an appropriate method, because changing the old batteries costs are relatively high. Especially in many cases, access to different sensors and actuators for battery change may not be easily feasible. There are different mechanisms for vibration energy harvesting including electrostatic and electromagnetic methods and use of piezoelectricity materials. [1, 2]

The performance of energy harvesting equipment depends on the type of materials used in them. Amongst energy harvesting different materials, piezoelectric materials are more applied and are more vastly common, for their capability to obtain higher power densities [2]. Due to high availability and high piezo constants, the PZT type of piezoelectric materials is preferred as well. Other materials are also used including PMN-PT, PZN-PT and PVDF.

[*] Corresponding author. Tel.: +98 21 77105105.
E-mail address: r.hosseini.mech@gmail.com (R.Hosseini).

By increasing width and thickness of beam, a higher output power can also be achieved [3]. Patel et al. [4] proposes a versatile model for optimizing the performance of a rectangular cantilever piezoelectric energy harvester. The model was used to investigate the effects of substrate and piezoelectric layer length, and piezoelectric layer thickness on the performance of a cantilever power scavenger. Findings from a parameter study indicate the existence of an optimum sample length due to increased mechanical damping for longer beams and improved power output using thicker piezoelectric layers. It is suggested that, in designing with the aim of generating more power, the following strategies be used: 1) for the beam, a shorter length, larger width, and lower ratio of piezoelectric layer thickness to total beam thickness are preferred in the case of a fixed mass; 2) for the mass, a shortened mass length and a higher mass height are preferred in the case of variation in the mass length and the mass height with mass width and mass value remain fixed, and a wider width and small mass height are preferred in the case of variation in mass width and height (mass length and value remain fixed; and 3) for the case of a fixed total length, a shorter beam length and longer mass length are preferred [5]. Beams deformed due to experiencing higher stresses, generate more output voltage [6]. Cantilever beams enjoy more advantages than other types of beams, because their deformation is more than other types of the beams and so they can produce more power density [7]. Cantilever beams are designed and manufactured in different rectangular, trapezoidal, triangular and *V*-shaped forms [8]. The relations required for resonance frequency calculations types of piezoelectric harvesters with common configurations have been presented in Ref [8] to facilitate the process of their design. On the micro scale, new forms of cantilever beams have also been studied, including the shell structure [9], spiral configuration [10] and zigzag [11] ones. Based on this, it is observed that there are different forms for cantilever beam optimization in terms of power generation. This paper fundamentally concentrates on design parameters and rates of harvested energy in a bimorph piezoelectric beam energy harvester. Motion equations have been obtained based on Euler-Bernoulli theory and the Finite Element (FE) simulation has been done using ABAQUS.

2 CANTILEVER BEAM FREE VIBRATIONS ANALYSIS

In this section, rectangular, trapezoidal and triangular beam natural frequencies have been estimated. For a uniform beam under free vibrations with no damping, motion equation is according to Eq. (1) [12, 13]

$$EI\frac{\partial^4 z(x,t)}{\partial x^4}+m\frac{\partial^2 z(x,t)}{\partial t^2}=f_0(x,t) \tag{1}$$

Coefficient *EI* shows beam stiffness, *m* equals to mass per unit length and *z* is indicative of beam transverse displacement in terms of location and time at the place of natural axis in a desirable section of the beam length. Beam transverse displace *z* is expressed using Eq. (2) [14]:

$$z(x,t)=z_b(x,t)+z_{rel}(x,t) \tag{2}$$

where $z_b(x,t)$ equals beam base displacement and $z_{rel}(x,t)$ indicates beam displacement relative to beam base.

2.1 Natural frequencies estimation for a rectangular beam

The schematic of the piezoelectric cantilever beam is shown in Fig 1. Using modal analysis technique, the response to free vibrations will be obtained as below:

$$z_{rel}(x,t)=\sum_{n=1}^{\infty} w_n(x)q_n(t) \tag{3}$$

where $w_n(x)$ and $q_n(t)$ are the state vector orthogonized mass and modal coordinates in the n^{th} mode, respectively [13]. By substituting Eq. (3) in (1), one will obtain:

$$\frac{EI}{mw_n(x)}\frac{d^4w_n(x)}{dx^4} = -\frac{1}{q_n(t)}\frac{d^2q_n(t)}{dt^2} = \omega_n^2 \tag{4}$$

where w_n is a positive constant value showing the harmonic response in the cantilever beam. The left hand term in Eq. (4) is simplified according to Eq. (5) as follows:

$$\frac{d^4w_n(x)}{dx^4} - \lambda_n^4 w_n(x) = 0 \tag{5}$$

where

$$\lambda_n^4 = \frac{m}{EI}\omega_n^2 \tag{6}$$

Assuming that $w_n(x) = Ce^{sx}$ where *C* and *s* are constant, the solution of Eq. (5) will be according to Eq. (7):

$$w_n(x) = C_1 \sin\left(\frac{\lambda_n}{L}x\right) + C_2 \cos\left(\frac{\lambda_n}{L}x\right) + C_3 \sinh\left(\frac{\lambda_n}{L}x\right) + C_4 \cosh\left(\frac{\lambda_n}{L}x\right) \tag{7}$$

where C_1 and C_4 are constants obtained based on boundary conditions. The cantilever beam natural frequencies in the n^{th} mode are obtained from Eq. (6), equaling:

$$\omega_n = \lambda_n^2\sqrt{\frac{EI}{mL^4}} \tag{8}$$

Since the cantilever beam in this study consists of two materials, terms *m* and *EI* will be according to Eqs. (9) and (10) [2]:

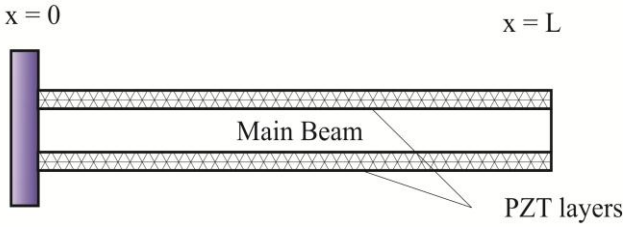

Fig. 1
Bimorph piezoelectric cantilever beam for vibration energy harvesting.

$$m = B(\rho_b h_b + \rho_p h_p) \tag{9}$$

$$EI = \frac{E_b B h_b^3 + E_p B(8h_p^3 + 6h_b^2 h_p + 12h_b h_p^2)}{12} \tag{10}$$

where *B* is cantilever width, ρ is cantilever density and *h* indicates cantilever thickness at different sections. Index *b* shows cantilever beam structure and ρ is relevant to the piezoelectric material. By applying boundary conditions to solve $w_n(x)$, the frequency equation will be obtained as below [13];

$$1 + \cos\lambda_n \cosh\lambda_n = 0 \tag{11}$$

where the values of λ_n for a cantilever beam have been listed in Table 1.

Table 1
Cantilever beam eigenvalues in different modes.

Node number	λ_n
1	1.875
2	4.6941
3	7.8547
4	10.9956

Eq. (7) will accordingly be in the form of Eq. (12)

$$w_n(x) = \cos\left(\frac{\lambda_n}{L}x\right) - \cosh\left(\frac{\lambda_n}{L}x\right) - \beta_n\left[\sin\left(\frac{\lambda_n}{L}x\right) - \sinh\left(\frac{\lambda_n}{L}x\right)\right] \tag{12}$$

where

$$\beta_n = \frac{\cos(\lambda_n) + \cosh(\lambda_n)}{\sin(\lambda_n) + \sinh(\lambda_n)} \tag{13}$$

Eq. (12) shows the n^{th} mode shape of the beam. More discussions about the natural frequency calculation of different cantilever geometries are found in [15-18].

2.2 Natural frequencies estimation for a nonrectangular cantilever beam

Assuming the constant mode shape obtained according to Eq. (12) in the previous part and using Rayleigh method [19], equations relevant to the natural frequencies can be developed. In this state, the cantilever beam width is a function of its length and defined according to Eq. (14).

$$B(x) = rB(0) + \frac{B(0)(1-r)}{L}(L-x) \tag{14}$$

where $B(0)$ is cantilever beam width in the part connected to the wall and r is the ratio of tapering and can written as $r = B(L)/B(0)$ (Fig. 2). According to Eq. (12) we have:

$$w_n(x,t) = \left[\cos\left(\frac{\lambda_n}{L}x\right) - \cosh\left(\frac{\lambda_n}{L}x\right) - \beta_n\left(\sin\left(\frac{\lambda_n}{L}x\right) - \sinh\left(\frac{\lambda_n}{L}x\right)\right)\right]\sin(\omega t + \alpha) \tag{15}$$

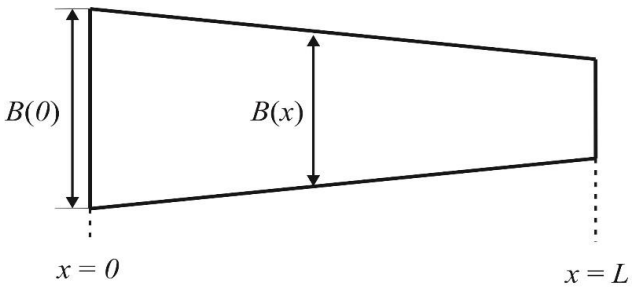

Fig. 2
Dimensions of the trapezoidal cantilever beam.

where α is a constant number and ω and t indicate the angular frequency and the time elapsed, respectively. In the general state, kinetic energy of the cantilever beam is obtained according to Eq. (16) as follows:

$$T = \int_0^L \frac{1}{2}(\rho_b h_b + 2\rho_p h_p) B(x) \left(\frac{\partial^2 w(x,t)}{\partial x^2} \right)^2 dx \tag{16}$$

On the other hand, the amount of potential energy is obtained based on Eq. (17)

$$U = \int_0^L \frac{1}{2} EI(x) \left(\frac{\partial^2 w(x,t)}{\partial x^2} \right)^2 dx \tag{17}$$

Based on the energy conservation low, thus the natural frequency will equal:

$$\omega_n = \sqrt{\frac{\left(\frac{\lambda_n}{L}\right)^4 \left[\frac{E_b h_b^3 + E_p (8h_p^3 + 6h_b^2 h_p + 12 h_b h_p^2}{12} \right] \int_0^L B(x) \left[\begin{array}{l} [-\cos\left(\frac{\lambda_n}{L} x\right) - \cosh\left(\frac{\lambda_n}{L} x\right)] \\ -\beta_n [-\sin\left(\frac{\lambda_n}{L} x\right) - \sinh\left(\frac{\lambda_n}{L} x\right)] \end{array} \right]^2 dx}{\left(\rho_b h_b + 2\rho_p h_p\right) \int_0^L B(x) \left[\begin{array}{l} [\cos\left(\frac{\lambda_n}{L} x\right) - \cosh\left(\frac{\lambda_n}{L} x\right)] \\ -\beta_n [-\sin\left(\frac{\lambda_n}{L} x\right) - \sinh\left(\frac{\lambda_n}{L} x\right)] \end{array} \right]^2 dx}} \tag{18}$$

It is noteworthy that in the design of energy harvesters, only the 1st mode is usually considered, based on which calculations will be made. For the resonance frequency calculation in order to design energy harvesters, simpler relations have been presented in Ref [8] for the structure resonance frequency initial estimation.

3 CANTILEVER BEAM FORCED VIBRATION ANALYSIS

In this part, the voltage generated due to the cantilever beam forced vibrations has been obtained, based on which, influenced by the cantilever base excitation, the motion equation will be according to Eq. (19)

$$\frac{\partial^2 M(x,t)}{\partial x^2} + m \frac{\partial^2 z_{rel}(x,t)}{\partial t^2} = -m \frac{\partial^2 z_b(x,t)}{\partial t^2} \tag{19}$$

where $M(x)$ is the bending moment. The stress-strain relation for the beam and piezoelectric layer is:

$$\sigma_1^b = E_b \varepsilon_2^b \tag{20}$$

$$\sigma_1^p = E_p (\varepsilon_1^p - d_{31} E_3) \tag{21}$$

where ε denotes cantilever beam strain and σ is the stress generated in the cantilever beam. d_{31} is the piezoelectricity module and E_3 is the electric field generated in the piezoelectric material. Based on the mode of piezoelectric layers connection and circuitry there will be two kinds of series and parallel connections in the circuit, shown in Fig 3.

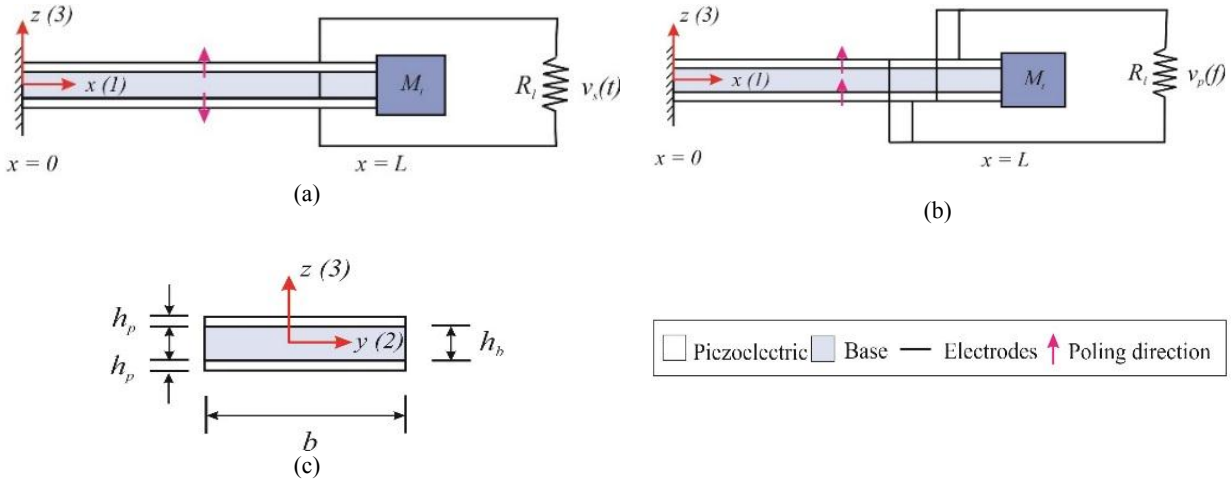

Fig. 3
a) Piezoelectric layers in series connection b) Piezoelectric layers in parallel connection c) Structure bimorph piezoelectric cross section.

In the piezoelectric series connection, the sign of d_{31} is opposite in the upper and lower piezoelectric layers (due to opposite polarities). Instantaneous electric fields are thus in the direction of each other and their amounts are computable in both layers using Eq. (22).

$$E_3(t) = -\frac{v(t)}{2h_p} \tag{22}$$

In the piezoelectric parallel connection, since the sign of d_{31} is the same in the upper and lower piezoelectric layers, instantaneous electric fields are in opposite directions, respectively calculated according to Eqs. (23) and (24) [2]

$$E_3(t) = -\frac{v(t)}{h_p} \tag{23}$$

$$E_3(t) = \frac{v(t)}{h_p} \tag{24}$$

The cantilever internal moment equals:

$$M(x,t) = -\int_{-(\frac{h_b}{2})-h_p}^{-(\frac{h_b}{2})} \sigma_1^p B y dy - \int_{-(\frac{h_b}{2})}^{(\frac{h_b}{2})} \sigma_1^b B y dy - \int_{(\frac{h_b}{2})}^{(\frac{h_b}{2})+h_p} \sigma_1^p B y dy \tag{25}$$

Here it is assumed that the width of the cantilever material and of the piezoelectric layer is the same, shown by B. The thickness of the cantilever beam and of the piezoelectric layer equals to h_b and h_p, respectively. Regarding the different output voltages in series and parallel connections, the piezoelectric coupling effect is expected to be different and displacement response $W_{rel}(x,t)$ is thus different in both states. If we show this value in the series and parallel connections by $z^S{}_{rel}(x,t)$ and $z^P{}_{rel}(x,t)$ respectively, the internal bending moment can be found from the following relations where indices S and P respectively refer to the piezoelectric layers in series and parallel connections.

$$M^s(x,t) = -EI\frac{\partial^z z^s_{rel}(x,t)}{\partial x^2} + \eta_b v_b(t)\left[H(x) - H(x-L)\right] \tag{26}$$

$$M^p(x,t) = -EI\frac{\partial^z z_{rel}^p(x,t)}{\partial x^2} + \eta_p v_p(t)\left[H(x) - H(x-L)\right] \tag{27}$$

where

$$\eta_b = \frac{E_2 B d_{31}}{2h_p}\left[\left(h_p + \frac{h_b}{2}\right)^2 - \frac{h_b^2}{4}\right] = E_2 B d_{31}\left(\frac{h_p + h_b}{2}\right) \tag{28}$$

$$\eta_p = 2\eta_b = E_2 B d_{31}(h_p + h_b) \tag{29}$$

L is cantilever beam total length. In the parallel connection state, by using Eq. (27) in (19) the mechanical equation of the cantilever beam motion with electric coupling will thus be obtained:

$$EI\frac{\partial^4 z_{rel}(x,t)}{\partial x^4} + m\frac{\partial^2 z_{rel}(x,t)}{\partial t^2} + \eta v(t)\times\left[\frac{d\delta(x)}{dx} - \frac{d\delta(x-L)}{dx}\right] = -m\frac{\partial^2 z_b(x,t)}{\partial t^2} \tag{30}$$

where $\delta(x)$ is Dirac delta function fulfilling Eq. (31).

$$\int_{-\infty}^{\infty}\frac{d^{(k)}\delta(x-x_0)}{dx^{(k)}}f(x)dx = (-1)^k\frac{d^{(k)}f(x_0)}{dx^{(k)}} \tag{31}$$

On the other hand, for obtaining electric equations, Eq. (32), used for piezoelectric materials has been applied.

$$D_3 = d_{31}\sigma_1 + \varepsilon_{33}^T E_3 \tag{32}$$

where D_3 is electric displacement, σ_1 is stress, ε_{33}^T is dielectric constant in constant stress and E_3 indicates uniform electric field. By changing Eq. (32), stress will be written in terms of the piezoelectric material Young module and strain. Since $\varepsilon_{33}^T = \varepsilon_{33}^S + d_{31}E_p$, by using Eqs. (31) and (32), we will have:

$$D_3 = d_{31}E_p\varepsilon_1(x,t) - \varepsilon_{33}^s\frac{v(t)}{h_p} \tag{33}$$

Electric potential q (t) in one of the piezoelectric layers can be obtained by integrating electric displacement on the piezo layer surface according to Eq. (34).

$$q(t) = \int\vec{D}_3.\vec{n}dA = -\int_{x=0}^{x=L}\left[d_{31}\left(\frac{h_b}{2} + h_p\right)E_p B\frac{\partial^z z_{rel}(x,t)}{\partial x^2} - \varepsilon_{33}^s B\frac{v(t)}{h_p}\right]dx \tag{34}$$

where $\vec{D}$ is electric displacement vector and n equals to unit vector normal to the surface. By differentiation $q(t)$ relative to time, the relation current will be obtained. Then:

$$i(t) = \int_{x=0}^{x=L}\left[d_{31}\left(\frac{h_b}{2} + h_p\right)E_p B\frac{\partial^3 z_{rel}(x,t)}{\partial x^2\partial t}\right]dx + \frac{\varepsilon_{33}^s BL}{h_p}\frac{dv(t)}{ht} \tag{35}$$

The 2nd term of Eq. (35) is for the piezoelectric material capacitor property. For convenience, the piezoelectric material can be connected to the resistance load which will function as the current source with no external capacitor element [2]. The output voltage will thus be obtained as follows:

$$v(t) = R_L i(t) = -R_L \int_{x=0}^{x=L} \left[d_{31} \left(\frac{h_b}{2} + h_p \right) E_p B \frac{\partial^3 z_{rel}(x,t)}{\partial x^2 \partial t} \right] dx + \frac{\varepsilon_{33}^s BL}{h_p} \frac{dv(t)}{ht} \tag{36}$$

where R_L is indicative of resistance due to load.

3.1 Estimation of the voltage generated in the rectangular cantilever

Eq. (19) is used for this purpose. According to modal analysis, we have:

$$EI \frac{\partial^4}{\partial x^4} \sum_{n=1}^{\infty} w_n(x) q_n(t) + m \frac{\partial^2}{\partial t^2} \left[\sum_{n=1}^{\infty} w_n(x) q_n(t) \right] + x_n v(t) = -m \frac{\partial^2 z_b(x,t)}{\partial t^2} \tag{37}$$

where

$$x_n = \eta \frac{dw_n(x)}{dx} \Big|_{x=L} \tag{38}$$

By multiplying both ends of Eq. (37) by mass normalized function $w_p(x)$ and integrating in the cantilever length, and using the orthogonality condition, the following result (Eq. (39)) will be obtained:

$$\frac{d^2 q_n(t)}{dt^2} + \omega_n^2 q_n(t) + x_n v(t) = -\int_0^L w_n(x) m \frac{\partial^2 z_b(x,t)}{\partial t^2} dx \tag{39}$$

For approximation to reality, the damping effect will also be added to equations [20] to obtain the following result (Eq. (40))

$$\frac{d^2 q_n(t)}{dt^2} + 2\xi_n \omega_n \frac{dq_n(t)}{dt} + \omega_n^2 q_n(t) + x_n v(t) = -\int_0^L w_n(x) \frac{\partial^2 z_b(x,t)}{\partial t^2} dx \tag{40}$$

with a little change in Eq. (36), we have:

$$\frac{dv(t)}{dt} + \frac{h_p}{\varepsilon_{33}^s BLR_L} v(t) = \frac{d_{31} E_p (h_b / 2 + h_p) h_p}{\varepsilon_{33}^s L} \int_0^L \frac{\partial^3 z_{rel}(x,t)}{\partial x^2 \partial t} dx \tag{41}$$

Using Eq. (3) in Eq. (4), the integral expression can be expressed as below:

$$\int_0^L \frac{\partial^3 z_{rel}(x,t)}{\partial x^2 \partial t} dx = \sum_{n=1}^{\infty} \frac{dq_n(t)}{dt} \int_0^L \frac{d^2 w_k(x)}{dx^2} dx = \frac{dq_n(t)}{dt} \frac{dw_n(x)}{dx} \Big|_{x=L} \tag{42}$$

In the end, Eq. (41) will be in the form of Eq. (43)

$$\frac{dv(t)}{dt} + \frac{h_p}{\varepsilon_{33}^s BLR_L} v(t) = \sum_{n=1}^{\infty} \varphi_n \frac{dq_n(t)}{dt} \tag{43}$$

where

$$\varphi_n(x) = -\frac{d_{31}E_p(h_b/2+h_p)h_p(t)}{\varepsilon_{33}^s}\frac{dw_n(x)}{dx}\Big|_{x=L} \tag{44}$$

Using the function in Eq. (45) for $v(t)$, Eq. (41) will be solved.

$$\psi(t) = e^{t/\tau_c} \tag{45}$$

where τ_c is the circuit time constant, defined as per Eq. (46):

$$\tau_c = \frac{\varepsilon_{33}^s BLR_L}{h_p} \tag{46}$$

The cantilever motion has been assumed to be harmonic. Given $z_b = Y_0 e^{i\omega t}$ and $v(t) = V_0 e^{i\omega t}$ in Eq. (40), $q_k(t)$ will be obtained according to Eq. (47):

$$q_n(t) = \frac{\left[m\omega^2 Y_0 \int_0^L w_n(x)dx - x_n V_0\right]e^{i\omega t}}{\omega_n^2 - \omega^2 + 2i\xi_n\omega_n\omega} \tag{47}$$

where ω is the excitation frequency and i is a unit imaginary number. On the other hand, based on Eq. (43), we have:

$$\left(\frac{1+i\omega\tau_c}{\tau_c}\right)V_0 e^{i\omega t} = \sum_{n=1}^{\infty}\phi_n\frac{dq_n(t)}{dt} \tag{48}$$

By substituting Eq. (47) in (48), the value of V_0, being indicative of the voltage vibrations amplitude, will be obtained based on Eq. (49)

$$\left(\frac{1+i\omega\tau_c}{\tau_c}\right)V_0 e^{i\omega t} = \sum_{n=1}^{\infty}\phi_n\frac{i\omega\left[m\omega^2 Y_0 \int_0^L w_n(x)dx - x_n V_0\right]e^{i\omega t}}{\omega_n^2 - \omega^2 + 2i\xi_n\omega_n\omega} \tag{49}$$

The ratio of the output voltage to the basement beam acceleration called Frequency Response Function (FRF) in every piezoelectric layers will thus equal:

$$\frac{v(t)}{\omega^2 Y_0 e^{i\omega t}} = \frac{\sum_{n=1}^{\infty}\frac{\phi_n i\omega m\left(\int_0^L w_n(x)dx\right)}{\omega_n^2 - \omega^2 + 2i\xi_n\omega_n\omega}}{\left(\sum_{n=1}^{\infty}\frac{i\omega\phi_k x_k}{\omega_n^2 - \omega^2 + 2i\xi_n\omega_n\omega}\right) + \frac{1+i\omega\tau_c}{\tau_c}} \tag{50}$$

3.2 Estimation of the voltage generated in the toothed rectangular cantilever beam

For a comb-shaped rectangular cantilever beam which is in effect a structure consisting of some rectangular cantilever beam, the response will be a voltage equaling total voltages of each of the individual cantilever beams, and thus:

$$\frac{v(t)}{\omega^2 Y_0 e^{i\omega t}} = \sum_{n=1}^{n_0} \frac{\sum_{n=1}^{\infty} \frac{\phi_n i\omega m\left(\int_0^L w_n(x)dx\right)}{\omega_n^2 - \omega^2 + 2i\xi_n\omega_n\omega}}{\left(\sum_{n=1}^{\infty} \frac{i\omega\phi_n x_n}{\omega_n^2 - \omega^2 + 2i\xi_n\omega_n\omega}\right) + \frac{1+i\omega\tau_c}{\tau_c}} \tag{51}$$

where *n* indicates cantilever beams used in the structure.

3.3 Estimation of the in voltage generated the toothed nonrectangular cantilever beam

Rectangular equations can also be applied to the nonrectangular cantilever beams. Yet, changes including *m* and *I(x)* (surface inertia) should be made in them, for in that case, contrary to the simpler rectangular cantilever beam, width will change along the cantilever beam length.

4 FINITE ELEMENT SIMULATION AND VERIFICATION OF RESULTS

In order to verify the obtained results, the results of finite element analysis and the experiment conducted in Ref [21] on a rectangular cantilever beam is compared. The mechanical properties and geometric parameters of this case study have been respectively stated in Tables 2 and 3. Experimental, analytical and numerical results are listed in Table 4. As observed, there is a good compliance between the results. It is of course worthy of mention that the damping effect has been ignored in the calculations, and it is expected that by considering this parameter, more precision will be achieved in the result. Finite element simulation made for rectangular cantilever beam is shown in Fig 4.

Table 2
Mechanical properties of piezoelectric material used for simulation.

Piezoelectric(PZT-5A)	Value	Brass(Sub layer)	Value
Elasticity module, E_p [N/m^2]	5.1e10	Elasticity module, E_p [N/m^2]	9.7e10
Density, ρ_p [kg/m^3]	7750	Density, ρ_p [kg/m^3]	8490

Table 3
Geometric parameters used in the cantilever beam structure applied for simulation and experiment.

Metal sublayer thickness (*mm*)	Piezoelectric material thickness (*mm*)	Width (*mm*)	Length (*mm*)
0.132	0.188	3.175	28.6

Table 4
Experimental, analytical and numerical results of the bimorph piezoelectric rectangular cantilever beam

Beam structure	Frequency (*Hz*)	Output voltage (*V*)
Experimental result	246	10.24
Finite element simulation	258.44	9.24
Analysis result	258.05	9.73

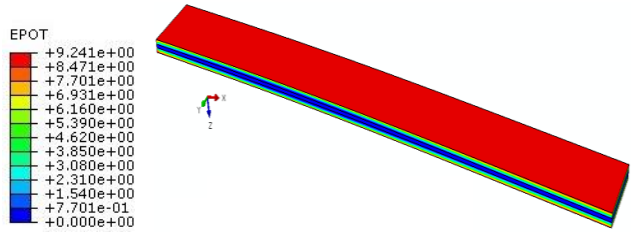

Fig. 4
Bimorph piezoelectric cantilever beam finite elements simulation.

In order to study the beam form effect, the ratio of the beam both ends has been considered in studies (Fig. 5). Ratio 1 denotes rectangular and 0 triangular beams.

Fig 6. Shows FE models for 3 states of rectangular, trapezoidal and triangular beams. Modelling has been made in ABAQUS and the results are shown in Fig. 7 for a point uniform loading. Simulation results show that under identical conditions, a triangular cantilever beam has optimized strain distribution and has made it more uniform.

Regarding calculations, mean strain in the triangular beam will be twice as high as in the rectangular beam. As the result of this strain distribution, the triangular beam provides more voltage and power than trapezoidal and rectangular beams do.

For different triangular functions *B(x)* applied in the analytic relations, for natural frequency and output voltage, these relations can also be extended to other geometries such as trapezoidal and triangular shapes.

Fig. 5
Beam both ends width.

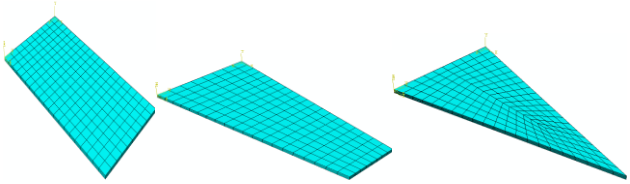

Fig. 6
Rectangular, trapezoidal and triangular piezoelectric cantilever beam harvester finite element models.

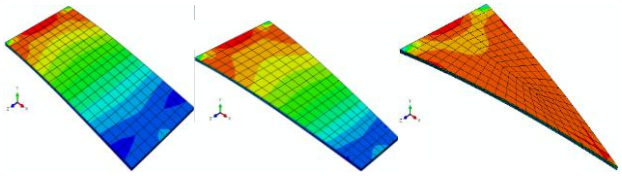

Fig. 7
Strain distribution in 3 different piezoelectric harvesters.

5 CONCLUSIONS

In this paper, analytical computations were made based on the distributed parameter model to extract the values of resonance frequency and output voltage of a bimorph piezoelectric cantilever beam which is the best and the simplest structure for application in energy harvesting systems. The equations were obtained based on Euler-Bernoulli beam and were calculated based on the system natural frequencies. The cantilever beam vibrations are based on the cantilever base excitation. Results from these equations and simulation and experimental results had much compliance with each other and these relations can be applied to design such harvesters.

From the strain field point of view, according to the finite element simulation, it was observed that under the effect of similar load for types of cantilever beams, with the beam deformation in a triangular state, the strain generated on the beam surface moves towards uniformity and in the triangular state, the mean strain will be twice as high as in the rectangular state and based on this, the generated voltage will also be higher.

REFERENCES

[1] Beeby S.P., Tudor M.J., White N., 2006, Energy harvesting vibration sources for microsystems applications, *Measurement Science and Technology* **17**: R175.

[2] Erturk A., Inman D.J., 2011, *Piezoelectric Energy Harvesting*, John Wiley & Sons.

[3] Jagtap S.N., Paily R., 2011, Geometry optimization of a MEMS-based energy harvesting device, *Students' Technology Symposium (TechSym)* **2011**: 265-269.

[4] Patel R., McWilliam S., Popov A.A., 2011, A geometric parameter study of piezoelectric coverage on a rectangular cantilever energy harvester, *Smart Materials and Structures* **20**: 085004.

[5] Zhu M., Worthington E., Tiwari A., 2010, Design study of piezoelectric energy-harvesting devices for generation of higher electrical power using a coupled piezoelectric-circuit finite element method, *IEEE Transactions on Ultrasonics, Ferroelectrics and Frequency Control* **57**: 427-437.
[6] Ayed S.B., Najar F., Abdelkefi A., 2009, Shape improvement for piezoelectric energy harvesting applications, *3rd International Conference, IEEE* **2009**: 1-6.
[7] Roundy S., Leland E.S., Baker J., Carleton E., Reilly E., Lai E., Otis B., Rabaey J.M., Wright P.K., Sundararajan V., 2005, Improving power output for vibration-based energy scavengers, *IEEE Pervasive Computing* **4**: 28-36.
[8] Hosseini R., Hamedi M., 2016, An investigation into resonant frequency of trapezoidal V-shaped cantilever piezoelectric energy harvester, *Microsystem Technologies* **22**: 1127-1134.
[9] Yang B., Yun K.-S., 2011, Efficient energy harvesting from human motion using wearable piezoelectric shell structures, *16th International Solid-State Sensors, Actuators and Microsystems Conference, IEEE* **2011**: 2646-2649.
[10] Hu H., Xue H., Hu Y., 2007, A spiral-shaped harvester with an improved harvesting element and an adaptive storage circuit, *IEEE Transactions on Ultrasonics, Ferroelectrics, and Frequency Control* **54**: 1177-1187.
[11] Karami M.A., Inman D.J., 2012, Parametric study of zigzag microstructure for vibrational energy harvesting, *Journal of Microelectromechanical Systems* **21**: 145-160.
[12] Thomson W., 1996, *Theory of Vibration with Applications*, CRC Press.
[13] Rao S.S., 2007, *Vibration of Continuous Systems*, John Wiley & Sons.
[14] Muthalif A.G., Nordin N.D., 2015, Optimal piezoelectric beam shape for single and broadband vibration energy harvesting: Modeling, simulation and experimental results, *Mechanical Systems and Signal Processing* **54**: 417-426.
[15] Hosseini R., Hamedi M., 2015, Improvements in energy harvesting capabilities by using different shapes of piezoelectric bimorphs, *Journal of Micromechanics and Microengineering* **25**:125008.
[16] Hosseini R., Hamedi M., 2015, Study of the resonant frequency of unimorph triangular V-shaped piezoelectric cantilever energy harvester, *International Journal of Advanced Design and Manufacturing Technology* **8**: 75-82.
[17] Hosseini R., Hamedi M., 2016, An investigation into resonant frequency of triangular V-shaped cantilever piezoelectric vibration energy harvester, *Journal of Solid Mechanics* **8**: 560-567.
[18] Hosseini R., Hamedi M., 2016, Resonant frequency of bimorph triangular V-shaped piezoelectric cantilever energy harvester, *Journal of Computational and Applied Research in Mechanical Engineering* **6**: 65-73.
[19] Yang K., Li Z., Jing Y., Chen D., Ye T., 2009, Research on the resonant frequency formula of V-shaped cantilevers, *4th IEEE International Conference on Nano/Micro Engineered and Molecular Systems*.
[20] Fakhzan M., Muthalif A.G., 2013, Harvesting vibration energy using piezoelectric material: Modeling, simulation and experimental verifications, *Mechatronics* **23**: 61-66.
[21] Ambrosio R., Gonzalez H., Moreno M., Torres A., Martinez R., Robles E., Sauceda A., Hurtado A., Heredia A., 2014, Study of cantilever structures based on piezoelectric materials for energy harvesting at low frequency of vibration, *Advanced Materials Research* **2014**: 159-163.